

Seismic Interferometry on background-noise field data

Deyan Draganov^{*,1}, Kees Wapenaar¹, Wim Mulder^{1,2}, and Johannes Singer²

(1) Delft University of Technology, Department of Geotechnique

Mijnbouwstraat 120, 2628RX Delft, The Netherlands

(2) Shell International E&P, Rijswijk, The Netherlands

Summary

Seismic Interferometry (SI) can construct reflection data from seismic background noise. In recent years, several authors developed the theory and applied it to synthetic data. With field data, the only success until now was the reconstruction of surface waves from coda and microseisms. Here, we attempt to reconstruct reflection events from noise data recorded in a desert area. The SI result shows inclined and horizontal coherent events. Some of the reconstructed events appear to align with reflections from an active survey. We cannot, however, exclude alternative explanations.

Introduction

Correlation of seismic observations at two receiver points with coordinates \mathbf{x}_A and \mathbf{x}_B reconstructs the Green's function between these two points, simulating a source in one and a receiver in the other point. This was proved first by Claerbout (1968) for a 1D acoustic medium. He showed that the autocorrelation of the observed transmission response produces the reflection response and named the method Acoustic Daylight Imaging. Later, he conjectured that crosscorrelation should also reconstruct the reflection response for 3D media. Wapenaar et al. (2002) and Wapenaar and Fokkema (2006) proved this concept for 3D inhomogeneous acoustic and elastic media using wave-equation reciprocity theorems of the correlation type. In recent years, the interest in this method has been steadily growing. To avoid confusion among similar techniques bearing different names and different techniques bearing similar names, the term Seismic Interferometry (SI) was selected for reconstruction through correlation, following the terminology of Schuster (2001). One application of SI is the reconstruction of seismic waves from seismic background noise that is otherwise discarded. Several authors have successfully reconstructed surface-wave arrivals between seismological stations from seismic coda and microseismic noise (e.g., Campillo and Paul (2003), Sabra et al. (2005) and Shapiro et al. (2005)). In this paper, we show results obtained from seismic background-noise data recorded in a quiet area. The aim of the experiment was to reconstruct reflection events.

Survey description

In 2005, Shell carried out a small field experiment in a desert area to test the applicability of the SI method for exploration purposes. The site was selected because cultural and man-made noise were minimal during the

nightly recordings and an active reflection survey, carried out during day-time, would allow for comparison. Seismic background noise was recorded by one line of seventeen 3C standard industry geophones, spaced at 50 meters. The sampling rate was 4 ms. As standard industry equipment was used, the maximum recording length was limited to 70 seconds, followed by a 30-second interruption to store the data. Because time series of the order of hours are required for the reconstruction of reflection data from background noise (Draganov et al., 2004), 523 recording intervals were combined to obtain about 10 hours of seismic background-noise data.

Processing results

For the application of SI to the acquired seismic background-noise data, we use the correlation equation

$$2\Re \left\{ \hat{G}_{p,q}(\mathbf{x}_A, \mathbf{x}_B, \omega) \right\} \hat{S}(\omega) \approx \frac{2}{\rho c_P} \left\langle \left\{ \hat{\nu}_p^{obs}(\mathbf{x}_A, \omega) \right\}^* \hat{\nu}_q^{obs}(\mathbf{x}_B, \omega) \right\rangle, \quad (1)$$

as derived in the frequency domain by Wapenaar and Fokkema (2006). $\hat{G}_{p,q}(\mathbf{x}_A, \mathbf{x}_B, \omega)$ represents the Green's function measured in the p -direction at \mathbf{x}_A at the free surface due to an impulsive source in the q -direction at the free surface at \mathbf{x}_B . $\hat{S}(\omega)$ is the power spectrum of the seismic background noise, \Re denotes the real part. The density in the subsurface is described by ρ and the propagation velocity for P-waves by c_P . The symbols $\hat{\nu}_p^{obs}(\mathbf{x}_A, \omega)$ and $\hat{\nu}_q^{obs}(\mathbf{x}_B, \omega)$ denote the observed particle velocity components in the p - and q -direction at \mathbf{x}_A and \mathbf{x}_B , respectively, due to a distribution of background-noise sources along an arbitrary shaped surface in the subsurface. The $\langle \cdot \rangle$ stands for spatial ensemble average. Equation 1 shows that we can reconstruct the particle velocity (the reflection response) and its time-reversed version at \mathbf{x}_A in the p -direction resulting from a traction source with spectrum $\hat{S}(\omega)$ at \mathbf{x}_B in the q -direction by correlating the recorded particle velocity components p and q observed, respectively, at the free-surface points \mathbf{x}_A and \mathbf{x}_B . The observed wavefields at \mathbf{x}_A and \mathbf{x}_B result from sources of seismic background noise present in the subsurface. The relationship was derived with the assumption that these sources are uncorrelated. When the subsurface sources of background noise illuminate the observation points from all directions, the reconstructed reflection response and its time-reversed version are symmetric and thus carry redundant information.

Following equation 1, we take the vertical particle veloc-

Seismic Interferometry on background-noise field data

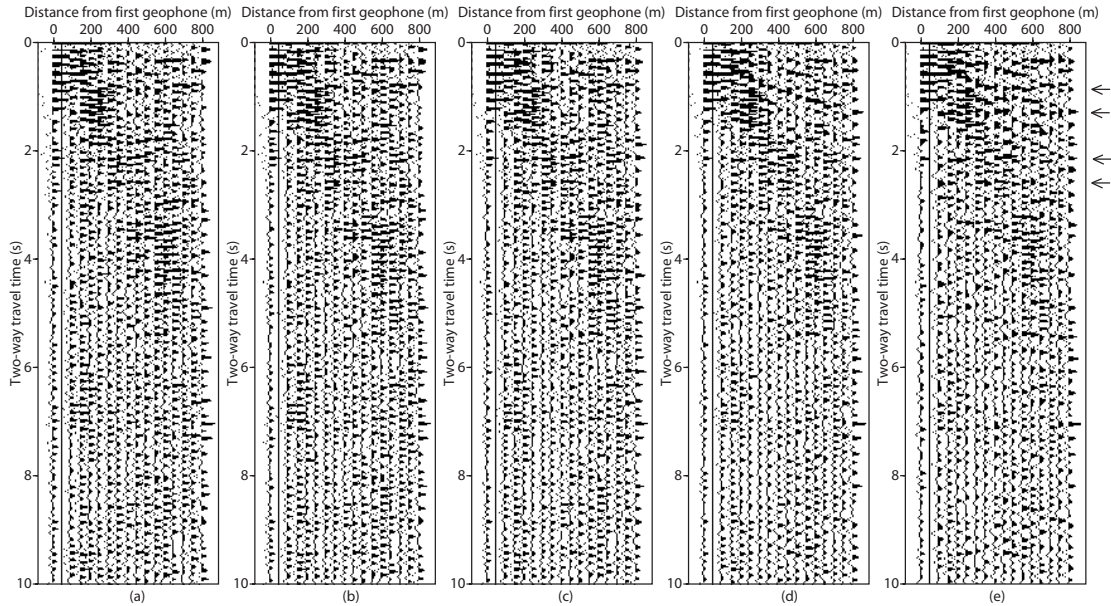


Fig. 1: Intermediate results from the process of building a reconstructed common-shot gather. The individual figures show the gradual reconstruction of the vertical particle velocity as if from a vertical traction source at $x_1 = 0$ m after summation of (a) 100, (b) 200, (c) 300, (d) 400 and (e) 500 correlation panels. We show here the first 10 s of the causal part of the correlation results. The arrows point to events that can be interpreted as nearly horizontal reflection arrivals. These arrivals will become clearer in the following figures.

ity component from the first recorded 70-second seismic background-noise panel. By choosing one of the traces as a master trace and correlating it with the other traces in the panel, we obtain a so-called correlation panel. We repeat the correlation operation for the second background-noise panel and add the result to the first correlation panel. This is repeated for all the seismic background-noise panels and the individual results are summed. The amplitude of the seismic background noise can vary significantly in the different panels. After crosscorrelation, this difference would be even bigger and after the summation process only a few correlation panels would contribute to the final result. To avoid this, we energy-normalize the individual seismic background-noise panels before correlation.

In this way, we reconstructed a reflection common-shot gather as if from a source at the position of the master trace and receivers at the positions of the other traces. Figures 1(a)–(e) show the gradual buildup of the final reconstructed common-shot gather by adding an increasing number of correlation panels. The results have been clipped to boost the later arrivals. As we used the vertical components of the seismic background-noise recordings, the figures show the gradual reconstruction of the vertical particle velocity that we would measure along the receiver positions when we would have a vertical traction source at $x_1 = 0$ m. It is clear that by adding additional correlation panels, we include more subsurface information and increase the signal-to-noise ratio. (In the original data, the trace at a horizontal distance of 50 m was dead.) Note the low-frequency nature of the data in Figure 1. The frequency spectra of the seismic background-noise panels showed that useful information lies mainly below 12 Hz.

For this reason, the data were band-pass filtered between 2 and 10 Hz after correlation. The subsurface geology in the area is composed of nearly horizontal layers. As we used only low frequencies, the reconstructed wavelet is wide (about 0.2 s). Because of this and because the receiver array had short offsets, reflection events in the reconstructed shot gathers should appear to have negligible moveout.

As mentioned above, the crosscorrelation reconstructs the reflection response (causal part) and its time-reversed version (anti-causal part), i.e., we obtain reflection events at positive as well as at negative times. The distribution of the seismic background-noise sources in the subsurface determines if reconstructed reflection events will appear in the causal and/or the anti-causal part of the correlation panel. As we do not know the source distribution, we should include both the causal and anti-causal parts of the final reconstructed shot gathers. Figure 2 shows the first 10 s of the causal (a) and the reversed-in-time anti-causal (b) parts of the final reconstructed common-shot gather obtained from the summation of 523 correlation panels. Figure 2(c) shows the sum of (a) and (b). The simulated shot is again positioned at a 0-m horizontal distance. The figure shows that some coherent events are reconstructed at positive and other at negative times. The summation of (a) and (b) should give us the full picture and should improve the signal-to-noise ratio. Figure 3 shows the reconstructed common-shot gathers after summing the causal and the anti-causal parts of the correlation panels when we would have a source at 150 m (a) and a source at 350 m (b). The processing that follows is applied to the summed causal and anti-causal parts of the reconstructed records.

Seismic Interferometry on background-noise field data

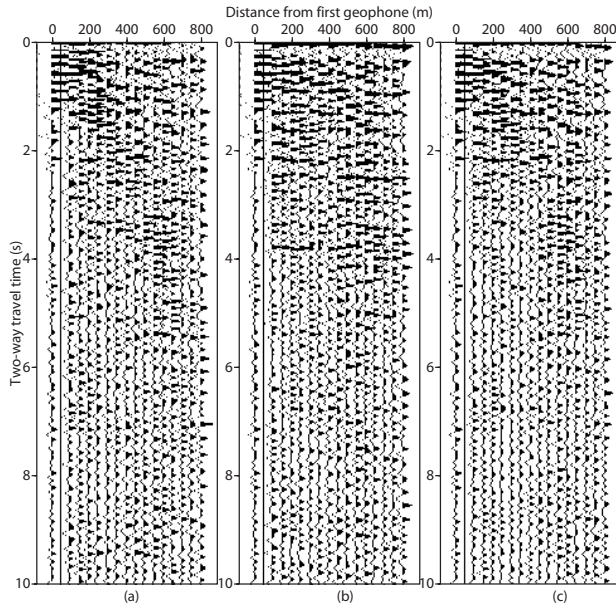


Fig. 2: Reconstructed vertical particle velocity reflection response as if from a vertical traction source at $x_1 = 0$ m. (a) Reconstructed coherent events in the causal part of the final correlation panel (positive times). (b) Reconstructed coherent events in the anti-causal part (negative times). (c) Result of the summation of (a) and (b).

By changing the position of the master trace along the receiver array, we have reconstructed common-shot gathers that simulate vertical traction sources at, respectively, $x_1 = 0, 100, 150, \dots, 800$ m. In theory, we could now perform velocity analysis on these shot gathers. In practice, this was difficult as moveout was nearly negligible because of the low frequencies used in the reconstruction and the short length of the receiver array. Another problem could be that when insufficient number of noise sources is present, the reconstruction process can produce incorrect coherent event. Nevertheless, the migration result from these reconstructions will still image correctly the subsurface (Draganov et al., 2004). We therefore took two other approaches. In the first one, we assume that the subsurface layering is flat. The common-shot gathers can then be stacked into a single common-offset panel. Note that the various reconstructed common-offset gathers may have widely different amplitudes. For this reason, we energy-normalized the individual common-offset gathers before stacking.

The second approach is a brute stack of the common-shot gathers (which simulates a plane-wave response). This will emphasize the nearly horizontal events, which can be attributed to deeper reflections or surface waves entering sideways. Random noise, shallow reflections, and surface waves will be suppressed. In each reconstructed common-shot gather, the reconstructed trace at the master-trace position will have a much higher amplitude than the rest of the traces. Again, before stacking, we energy-normalized the reconstructed common-shot gathers to

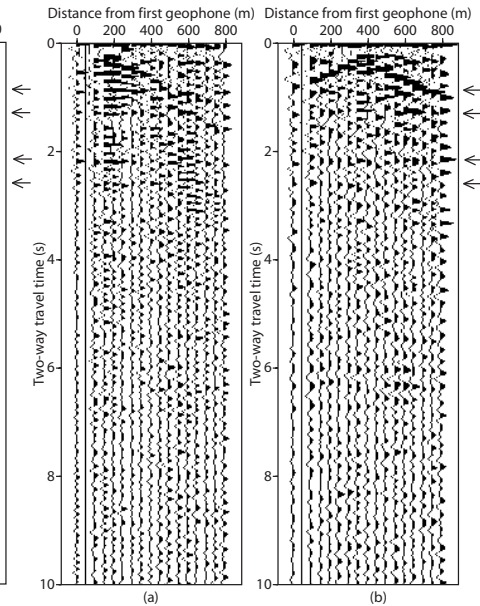


Fig. 3: (a) Reconstructed vertical particle velocity reflection response as if from a vertical traction source at $x_1 = 150$ m after summing the causal and the anti-causal parts. (b) Same as (a) but for a source at $x_1 = 350$ m.

make every trace count. Figure 4(a) shows the result after stacking into a common-offset gather, after normalizing for the different number of contributing traces and summing the corresponding negative and positive offset values. Offsets larger than 650 m were discarded. Several coherent events appear now more clearly against the noise that is still present. Some of these could already be discerned in the common-shot gathers. Figure 4(e) shows a common-offset panel produced from numerical modeling using a 1D elastic subsurface model derived from the active survey. (Note that this modeling result is used only to show that the reflection events for these low frequencies and short offsets should arrive nearly horizontal. The modeling should not be used to compare arrival times.) We might interpret the inclined events as surface waves and the horizontal events as reflections or multiples of reflections. However, surface waves that come in with a wavefront more or less parallel to the receiver array will have a similar character. The brute stack of each common-shot gather is displayed in Figure 4(b). Distance is now determined by the position of the original master trace. The stack suppresses inclined events.

Because we succeeded in bringing out some events, we are now in a position to make a comparison with the active data. Figures 4(c) and (d) show the result of Post-Stack Time-Migration (PSTM) for one line of the active survey that coincided with the passive array, but covering a much larger distance. The migration result extends to 6 s. We zero-padded to 10 s and low-pass filtered to 20 Hz to facilitate the comparison. In spite of the difference in

Seismic Interferometry on background-noise field data

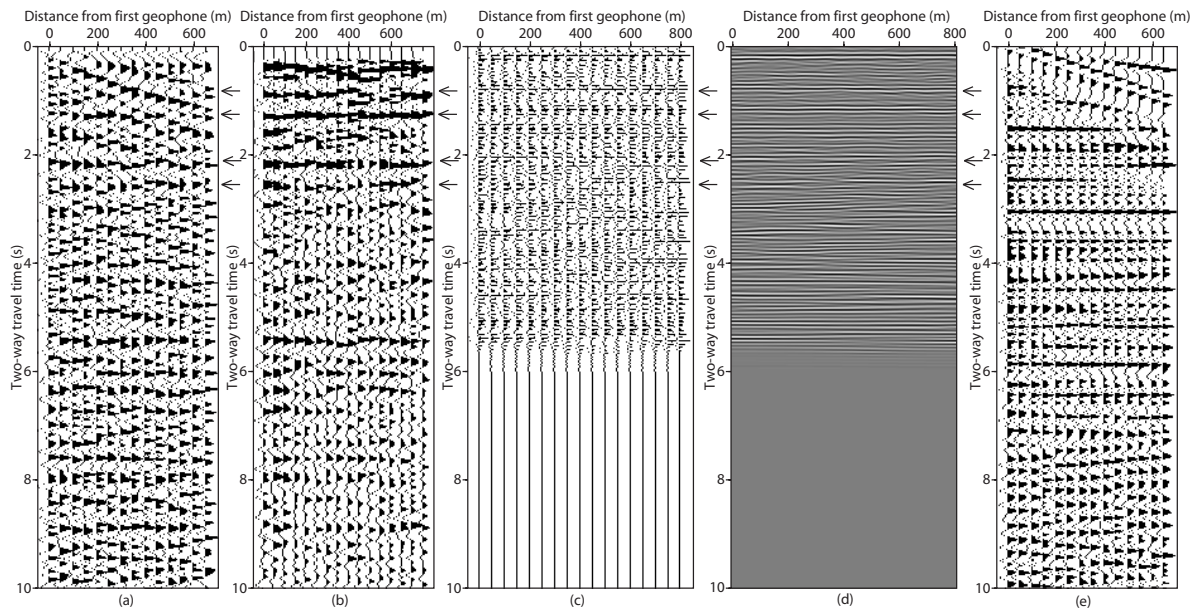


Fig. 4: (a) First ten seconds of a common-offset panel obtained by stacking all the reconstructed shot gathers. (b) First ten seconds of a brute stack of each shot gather. (c) Wiggle plot of the Post-Stack Time-Migration result from an active reflection survey in the same area (low-pass filtered up to 20 Hz). (d) Same as (c) but in a gray-scale plot. (e) Common-offset panel produced from finite-difference modeling using a 1D elastic subsurface model taken from the active survey. After 4 seconds, artefacts appear that are caused by the absorbing boundary conditions. This modeling result is included to show the shape of the expected coherent arrivals and should not be used for travel-time comparison.

frequency content, 2 to 10 Hz for the passive data and 10 to 20 Hz for the PSTM image, we observe a number of horizontal events in Figures 4(a) and (b) that align with 4(c) and/or (d). They occur at about 0.9 s, 1.3 s, 2.2 s, and 2.5 s (pointed out by the arrows) and perhaps also at 5.4 s. The last event was not visible on the reconstructed shot gathers, but was brought out by both the common-offset and the brute stack. Note that there are well-defined later events in (a) and (b). If they are caused by deeper reflections, they could give complementary information to the active survey.

Conclusions

We applied Seismic Interferometry to ten hours of passively acquired seismic background-noise data. The cross-correlation produced coherent events in the reconstructed shot gathers for sufficiently long recording time. Coherent arrivals appeared in the causal as well as in the anticausal part of the reconstructed shot gathers. The cross-correlation results were band-pass filtered between 2 and 10 Hz. Because of these low frequencies and because of the short length of the recording array, deeper reflection events had hardly any moveout. As the geology in the area is nearly horizontally layered, we stacked the reconstructed shot gathers into a single common-offset panel. This produces inclined events that might be attributed to surface waves, and nearly horizontal events that might be interpreted as deeper reflections. We also performed a brute stack of each shot gather. The latter suppressed events such as surface waves and further improved the signal-to-noise ratio. Both approaches produced coherent horizontal events. Because such events can be attributed not only to reflections, but also to multiples of reflections, to surface waves with a wavefront more or less parallel to the receiver array, and to other causes, we made a compar-

ison to active data recorded in the same area. A number of horizontal events from the passive experiment could be aligned with reflectors in the Post-Stack Time-Migration section. We cannot, however, exclude alternative explanations.

Acknowledgments

This research is supported by The Netherlands Research Centre for Integrated Solid Earth Sciences ISES, by the Technology Foundation STW, applied science division of NWO, and the technology program of the Ministry of Economic Affairs (grant DTN4915). The authors would like to thank Arie Verdel, Fons Ten Kroode, and Gerard Herman for the helpful discussions.

References

- Campillo, M. and A. Paul, 2003, Long-range correlations in the diffuse seismic coda: *Science*, 299, 547–549.
- Claerbout, J. F., 1968, Synthesis of a layered medium from its acoustic transmission response: *Geophysics*, 33, 264–269.
- Draganov, D., C. P. A. Wapenaar, B. Artman, and B. Biondi, 2004, Migration methods for passive seismic data: 74th Annual International Meeting, SEG, Expanded abstracts, 1123–1126.
- Sabra, K. G., P. Gerstoft, P. Roux, W. A. Kuperman, and M. C. Fehler, 2005, Extracting time-domain Green’s function estimates from ambient seismic noise: *Geophysical Research Letters*, 32, 10.1029/2004GL021862.
- Schuster, G. T., 2001, Theory of daylight/interferometric imaging: tutorial: 63th Conference and Exhibition, EAGE, Extended abstracts, A–32.
- Shapiro, N. M., M. Campillo, L. Stehly, and M. H. Ritzwoller, 2005, High-resolution surface wave tomography from ambient seismic noise: *Science*, 307, 1615–1618.
- Wapenaar, C. P. A., J. W. Thorbecke, D. Draganov, and J. T. Fokkema, 2002, Theory of acoustic daylight imaging revisited: 72nd Annual International Meeting, SEG, Expanded abstracts, ST 1.5.
- Wapenaar, C. P. A. and J. Fokkema, 2006, Green’s functions representations for seismic interferometry: *Geophysics*, in press.